● **RESEARCH ARTICLE**

Hyperhomocysteinemia induces injury in olfactory bulb neurons by downregulating Hes1 and Hes5 expression
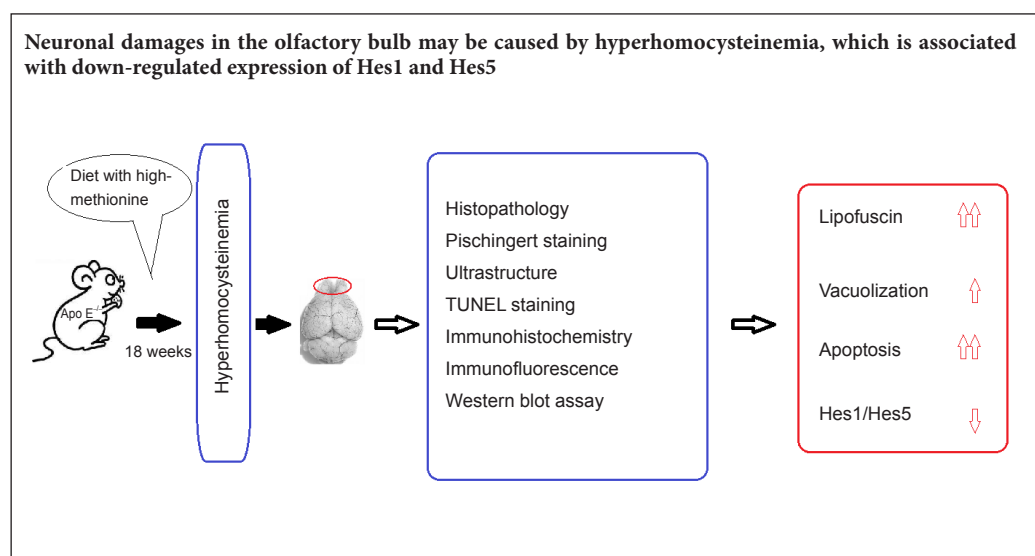
Jing-wen Zhang[1, 2, #], Bo Pang[1, #], Qi Zhao[1, #], Yue Chang[1], Yi-li Wang[2, *], Yi-deng Jiang[1], Li Jing[1, *]

1 School of Basic Medical Science, Ningxia Key Laboratory of Cerebrocranial Diseases-Incubation Base of National Key Laboratory, Ningxia Medical University, Yinchuan, Ningxia Hui Autonomous Region, China
2 Institute of Immunopathology, Medical School, Key Laboratory of Biomedical Information Engineering of Ministry of Education, Xi'an Jiaotong University, Xi'an, Shaanxi Province, China

Graphical Abstract

Neuronal damages in the olfactory bulb may be caused by hyperhomocysteinemia, which is associated with down-regulated expression of Hes1 and Hes5

*Correspondence to:
Yi-li Wang or Li Jing,
wangyili@mail.xjtu.edu.cn or
jingli@nxmu.edu.cn.

#These authors contributed equally to the study.

orcid:
0000-0003-2233-5453
(Li Jing)

Abstract

Hyperhomocysteinemia has been shown to be associated with neurodegenerative diseases; however, lesions or histological changes and mechanisms underlying homocysteine-induced injury in olfactory bulb neurons remain unclear. In this study, hyperhomocysteinemia was induced in apolipoprotein E-deficient mice with 1.7% methionine. Pathological changes in the olfactory bulb were observed through hematoxylin-eosin and Pischingert staining. Cell apoptosis in the olfactory bulb was determined through terminal deoxynucleotidyl transferase-mediated dUTP nick end-labeling (TUNEL) staining. Transmission electron microscopy revealed an abnormal ultrastructure of neurons. Furthermore, immunoreactivity and expression of the hairy enhancer of the split 1 (Hes1) and Hes5 were measured using immunohistochemistry, immunofluorescence, and western blot assay. Our results revealed no significant structural abnormality in the olfactory bulb of hyperhomocysteinemic mice. However, the number of TUNEL-positive cells increased in the olfactory bulb, lipofuscin and vacuolization were visible in mitochondria, and the expression of Hes1 and Hes5 decreased. These findings confirm that hyperhomocysteinemia induces injury in olfactory bulb neurons by downregulating Hes1 and Hes5 expression.

Key Words: nerve regeneration; olfactory bulb; apoptosis; neurons; Nissl body; homocysteine; hairy enhancer of split 1; hairy enhancer of split 5; neural regeneration

Introduction

Homocysteine (Hcy), a non-essential amino acid in humans, contains sulfur and is an intermediate product in methionine and cysteine biosynthesis (Ganguly and Alam, 2015; Xu et al., 2017). Under physiological conditions, blood contains a certain amount of Hcy. Hyperhomocysteinemia (HHcy), a common metabolic abnormal condition occurs because of an abnormal elevation in blood Hcy (Ganguly

and Alam, 2015; Xu et al., 2017). Epidemiological and clinical studies have suggested that HHcy is an independent risk factor for cardiovascular and cerebrovascular diseases and may be associated with neurodegenerative diseases, such as Alzheimer's disease, Parkinson's disease, brain atrophy, and epilepsy (Ganguly and Alam, 2015; Qasim et al., 2016; Reule et al., 2017). The mechanisms of disease and HHcy-induced lesions remain unclear. Elevated Hcy is suggested to act as

excitatory amino acids to increase the sensitivity of neurons to exogenous harmful substances and oxidative damage (Ganguly and Alam, 2015; Kamat et al., 2016; Qasim et al., 2016). Mildly elevated Hcy induces toxic effects on neuron-like cells (Curro et al., 2014). However, histological or cytological evidence demonstrates HHcy-induced damage in the central nervous system. The cytotoxic effect of neuronal damage and related molecular mechanisms require further research. Furthermore, the control or therapeutic interference of this disorder would facilitate the understanding of mechanisms underlying HHcy-induced brain lesions.

Recent studies have reported that the Notch signaling pathway maintains the proliferative capacity of cultured neuronal stem cells (Fortini, 2009; Del Debbio et al., 2010). Hairy enhancer of split 1 (Hes1), an important member of the aforementioned pathway, contains 282 amino acids (molecular weight: 29.6 kDa) (Katoh and Katoh, 2007). The activation of Hes1 can maintain the undifferentiated status of various precursor cells and ensure appropriate differentiation (Katoh and Katoh, 2007; Del Debbio et al., 2010; Imayoshi et al., 2010). Abundant Hes1 expression ensures the differentiation of brain functional cells, as well as regulates the number and proportion of neurons and glial cells (Katoh and Katoh, 2007; Imayoshi et al., 2010). The Hes1 and Hes5 defect could result in neuronal stem cells being unable to maintain their undifferentiated state, resulting in various abnormalities in the cell morphology and brain structure (Katoh and Katoh, 2007; Nichol et al., 2010). In adults, increased Hes1 protein expression is required to renew the proliferation of resting-stage and stem cells (Katoh and Katoh, 2007; Imayoshi et al., 2010). Hes1 expression has been reported to be involved in nervous regeneration and repair potential (Katoh and Katoh, 2007; Del Debbio et al., 2010; Imayoshi et al., 2010). However, the factors and mechanisms underlying Hes1 and Hes5 expression remain unknown. In addition, no study has demonstrated whether HHcy inhibits Hes1 and Hes5 expression and induces neuronal damage.

The olfactory bulb is established as an important part of the brain in mammals and is mainly composed of neurons, namely two main types of projection/sensory neurons and interneurons, glial cells, and nerve fibers (Lledo et al., 2008; Fletcher et al., 2009). Glutamic acid acts as a neurotransmitter in the projection neurons, such as mitral or glomerular cells. Most interneurons in the olfactory bulb use gamma-aminobutyric acid as a neurotransmitter (Gall et al., 1987; Fletcher et al., 2009). Early-stage neurological diseases induce neuronal damages in the olfactory bulb, the most important sensory organ in the brain, and olfactory dysfunction is typically preceded by cognitive impairment (Graves et al., 1999; Velayudhan et al., 2013). However, the effects of HHcy on the neuronal structure and Hes1 and Hes5 expression in the olfactory bulb have not been demonstrated.

Elevated Hcy can increase the sensitivity of neurons to injury because Hcy is affected as the excitatory amino acid (Wang et al., 2012; Ganguly and Alam, 2015). We hypothesize that neuronal damages in the olfactory bulb are caused by HHcy, which is associated with the downregulation of Hes1 and Hes5. In this study, HHcy was induced in apolipoprotein E-deficient (ApoE$^{-/-}$) mice by feeding them a high-methionine diet (Aléssio et al., 2011). We observed the injury in olfactory bulb neurons and the expression of Hes1 and Hes5 through histology, transmission electron microscopy, histochemistry, terminal deoxynucleotidyl transferase-mediated dUTP nick end-labeling (TUNEL), immunohistochemistry, immunofluorescence, and western blot assay.

Materials and Methods

Animals
Thirty-six male C57BL/6J mice with ApoE$^{-/-}$ (age: 5 weeks and weight: 18–20 g) were purchased from Jackson Laboratories (Bar Harbor, ME, USA). Male C57BL/6J mice ($n = 12$) with wild-type (Wt) Apo E (age: 5 weeks and weight: 18–20 g) were supplied by the Experimental Animal Center of Ningxia Medical University, Ningxia, China (licence No. SYXK (Ning) 2005-0001). All animal use and study protocols were in strict accordance with the Chinese Laboratory Animal Use Regulations. Efforts were made to minimize animal stress and reduce the number of mice used in this study. The animal studies were approved by the Ethical Committee of Ningxia Medical University (approval No. 2015-100).

Groups and intervention
The ApoE$^{-/-}$ mice with a high-methionine diet were used for HHcy models, as previously described (Aléssio et al., 2011; Jiang et al., 2012). After 1 week of acclimatization, the mice were randomly divided into four groups: (1) Wt control group (Wt group, $n = 12$), fed with a general diet (AIN-93G; Shanghai Saab Biological Co., Ltd., Shanghai, China); (2) ApoE$^{-/-}$ control group (ApoE$^{-/-}$ group, $n = 12$), fed with AIN-93G; (3) ApoE$^{-/-}$ with HHcy group (HHcy group, $n = 12$), fed with high-methionine diet (AIN-93G + 1.7% methionine); and (4) HHcy treated with folic acid and vitamin B12 group (HFB group, $n = 12$), fed with AIN-93G supplemented with 1.7% methionine, 0.006% folic acid, and 0.0004% vitamin B12. All mice were fed under the same conditions for 18 weeks at room temperature (22 ± 1°C) and humidity of 40–70% in a 12-hour light:dark cycle, and allowed food and water *ad libitum*.

Plasma Hcy determination
Under anesthesia with 3.5% chloral hydrate (0.1 mL/10 g), blood was collected from the eye and placed in EDTAK3 tubes at the end of 18 weeks treated with high methionine. The blood was allowed to stand at room temperature for 30 minutes. Plasma was then collected through centrifugation at 4°C and 3,000 r/min and stored below −80°C. Plasma total Hcy (tHcy) concentrations ($n = 12$, each group) were measured through high-performance liquid chromatography (Model-L2000; Hitachi, Tokyo, Japan).

Specimen preparation
Under anesthesia with 3.5% chloral hydrate (0.1 mL/10 g), the olfactory bulbs (Lledo et al., 2008) were divided into two sections along the sagittal section. The left hemispheres were

transferred to 4% paraformaldehyde for histopathology, Pischingert staining, TUNEL, immunohistochemistry, and immunofluorescence (n = 12 per group) and fixed overnight. Furthermore, the right hemispheres were sectioned to a thickness of 2 mm and glutaraldehyde-fixed for electron microscopy (n = 4 per group). The remaining tissue was frozen at −80°C for western blot assay (n = 8 per group).

Histopathological observation

The sections (thickness: 4 μm) were prepared from paraffin-embedded blocks for hematoxylin-eosin staining. The images, without overlapping, of the olfactory bulb were captured using a light microscope (DM4000 LED; Leica, Wetzler, Germany). The number of neurons, mitral cells, and granule cells per high-power field (400×) were counted and analyzed with Leica Application Suite 4.5 (Leica). Histopathological changes, such as necrosis and edema, were compared based on the histology of the Wt group using the double blind method.

Pischingert staining

The sections were dewaxed and hydrated, after a 10-minute incubation in methylene blue at room temperature. The sections were washed in phosphate-buffered saline (PBS; pH 4.6) until the Nissl bodies became clear. The sections were subsequently incubated with 4% ammonium molybdate buffer for 5 minutes. The images were observed and captured. The integrated optical density was analyzed with Leica Application Suite 4.5 (Leica), and the mean optical density was calculated by (integrated optical density sum)/area.

Transmission electron microscopy

Three sections (size: approximately $1 \times 1 \times 2$ mm^3) were removed from the freshly extracted right hemisphere of the olfactory bulb along the sagittal plane. The samples were transferred to 3% glutaraldehyde and fixed overnight at 4°C. Thereafter, they were washed three times with PBS (pH 7.4), followed by incubation in 1% osmium acid at room temperature for 2 hours for secondary fixation. The samples were then subjected to gradient acetone dehydration, epoxy resin 618 penetration, and embedding. For localization, a 1-μm section was stained with toluidine blue and observed through light microscopy (DM4000 LED; Leica). Furthermore, a 60-nm thick section was imaged through electron microscopy after dyeing. The ultrastructural changes in the neurons were analyzed through transmission electron microscopy (H7800; Hitachi). Mitochondrial vacuolization was defined as vacuolar structures with an expanded volume and cristae loss of more than 50%. Lipofuscin was defined as vacuolar structures containing electron-dense materials and autophagic vacuoles (Tyagi et al., 2010). The ratios of the neurons with mitochondrial vacuolization and lipofuscin were analyzed using the formula: numbers of neurons with mitochondrial vacuolization or lipofuscin/numbers of neurons with and without mitochondrial vacuolization or lipofuscin.

TUNEL staining

Apoptotic cells were detected using a TUNEL apoptosis detection kit (Zymed, San Diago, CA, USA) according to the manufacturer's instructions. The cells were stained with 3,3′-diaminobenzidine. The number of TUNEL-positive neurons per high-power field was counted and analyzed with Leica Application Suite 4.5 (Leica). Five fields were analyzed on each slide. The average ratio of TUNEL-positive cells per high-power field (400×) was calculated by numbers of TUNEL-positive cells/numbers of total cells.

Immunohistochemistry and immunofluorescence

The dewaxed and hydrated sections were soaked in 3% H$_2$O$_2$ to neutralize the endogenous peroxidase. To inhibit nonspecific binding, the sections were incubated in 10% goat serum at room temperature for 30 minutes. Subsequently, the sections were incubated in primary antibody anti-Hes1 polyclonal antibody (1:200, rabbit anti-mouse; Millipore, Shanghai, China) and anti-Hes5 polyclonal antibody (1:200, rabbit anti-mouse; Millipore) overnight at 4°C. The slices were incubated with horseradish peroxidase-conjugated immunoglobulin G (1:3,000, goat anti-rabbit; Sigma, St. Louis, MO, USA) at 37°C for 1 hour. The peroxidase complex was then incubated with 3,3′-diaminobenzidine. Images were obtained with an optical microscope (DM4000 LED; Leica). The number of Hes1- and Hes5-positive cells per high-power field (400×) was calculated and analyzed using Leica Application Suite 4.5 (Leica). The average ratio of Hes1- and Hes5-labeled neurons per high-power field was calculated by numbers of Hes1 and Hes5-labeled cells/numbers of total cells.

Immunofluorescence was performed using a previous protocol with modification (Jing et al., 2013), Briefly, the sections were blocked with 3% bovine serum albumin and subsequently incubated at 4°C overnight with anti-Hes1 and Hes5 polyclonal antibody (1:100, rabbit anti-mouse; Millipore). The sections were incubated with TRITC-labeled secondary antibody (1:100, goat anti-rabbit; Sigma) and observed using a fluorescence confocal scanning microscope (FV100 IX81; Olympus, Tokyo, Japan). The Hes1- and Hes5-positive neuronal cells per high-power field (400×) in the images were counted using Leica Application Suite 4.5 (Leica).

Western blot assay

The olfactory bulbs were homogenized in ice-cold lysis buffer. The protein concentration was measured using the bicinchoninic acid assay kit (Thermo Scientific, Shanghai, China), according to the manufacturer's instructions. Proteins were separated through 8%, 10%, and 15% sodium dodecylsulfate-polyacrylamide gel electrophoresis and then transferred to nitrocellulose membranes. The membranes were incubated in 10% skim milk for 1 hour and incubated overnight with Hes1 and Hes5 polyclonal antibodies (1:3,000, rabbit anti-mouse; Millipore) or rabbit anti-mouse glyceraldehyde-3-phosphate dehydrogenase (1:1,000; Sigma). The membranes were then washed with Tris-buffered saline/

Tween and incubated with horseradish peroxidase-labeled secondary antibody (1:3,000, goat anti-rabbit; Sigma) at room temperature for 1 hour. The enhanced chemiluminescence solution (Abcam, Cambridge, UK) was used to detect the proteins. The bands were visualized on an X-ray film. Band densitometry was measured using the Gene Genius Gel Imaging System (Bio-Rad, Cambridge, UK). The relative gray values were calculated after normalization to the loading control.

Statistical analysis
Data are expressed as the mean ± SD. Statistical analysis was performed using one-way analysis of variance with SPSS 20.0 (IBM, Armonk, NY, USA). Tukey's *post-hoc* test was used for multiple comparisons. The unpaired *t*-test was used between two groups. $P < 0.05$ was considered statistically significant.

Results

Plasma tHcy increases in HHcy mice
In the Wt group, the plasma tHcy level was 3.24 µM. This level was normal in the ApoE$^{-/-}$ group. The plasma tHcy level increased significantly (HHcy level) in the HHcy group compared with the Wt and ApoE$^{-/-}$ groups ($P < 0.05$). The plasma tHcy levels were significantly lower in the HFB group (normal level) than in the HHcy group ($P < 0.05$), but were higher than those in the Wt and ApoE$^{-/-}$ groups ($P < 0.05$; **Figure 1**).

Histological changes in the olfactory bulb of HHcy mice
In each group, we could observe the basic structure of the olfactory bulb (**Figure 2A**), namely the olfactory nerve, synaptic sphere, external plexiform, mitral cell, internal plexiform, and granule cell layers. Compared with Wt, ApoE$^{-/-}$, and HFB groups, no significant decrease in the cell number, as indicated by mitral and granule cells, was observed in the HHcy group ($P > 0.05$; **Figures 2A, C**). The Nissl body, which was abundant in mitral and granule cells, was visualized through Pischingert staining (**Figure 2B**), Furthermore,
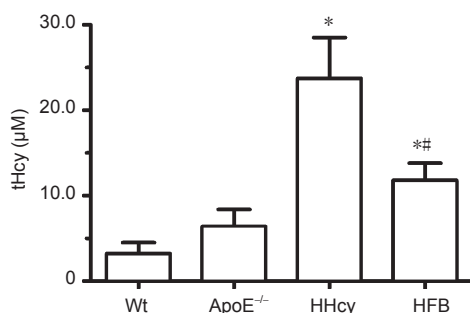

Figure 1 Plasma tHcy levels in HHcy mice.
Data are expressed as the mean ± SD (n = 12), analyzed by one-way analysis of variance followed by Tukey's *post-hoc* test for multiple comparisons. The unpaired *t*-test was used between two groups. ∗$P < 0.05$, *vs.* Wt and ApoE$^{-/-}$ groups, respectively; #$P < 0.05$, *vs.* HHcy group. tHcy: Total homocysteine; HHcy: hyperhomocysteinemia; ApoE$^{-/-}$: apolipoprotein E-deficient.

no significant difference was observed in the mean optical density after Pischingert staining in all study groups ($P > 0.05$; **Figure 2C**).

Changes in neuronal ultrastructure of the olfactory bulb of HHcy mice
To understand the early damage induced by HHcy in cell structures, such as mitochondria and endoplasmic reticulum, we observed the cells through transmission electron microscopy. The ultrastructural observation revealed no obvious abnormalities in the cell structure, such as the membrane, cytoplasm, and nucleus of the mitral cells in the olfactory bulb in all study groups. In the Wt (**Figure 3A**) and ApoE$^{-/-}$ groups (**Figure 3B**), normal mitochondria, rough endoplasmic reticulum, and abundant ribosomes were visible. Furthermore, in the HHcy group, increased mitochondrial vacuolization and lipofuscin were observed (**Figure 3C**). In the HFB group, in addition to ribosome reduction, lump formation of early lipofuscin in the mitochondrial cavity was observed (**Figure 3D**). Compared with the Wt, ApoE$^{-/-}$, and HFB groups, the HHcy group showed significantly increased numbers of neurons with mitochondrial vacuolization and lipofuscin ($P < 0.05$; **Figure 3E**).

Apoptosis in the olfactory bulb of HHcy mice
Apoptosis of cells in the olfactory bulb was assessed through TUNEL staining. A few TUNEL-positive cells were scattered in the granule cell layer of the olfactory bulb in the Wt (**Figure 4A**) and ApoE$^{-/-}$ (**Figure 4B**) groups. The apoptotic cells were significantly increased in the HHcy group (**Figure 4C**). However, treatment with folic acid and vitamin B12 inhibited the increase in apoptosis under a high-methionine diet (**Figure 4D**). The number of TUNEL-positive cells in the HHcy group was significantly increased ($P < 0.05$), and this number in the HFB group was significantly lower than that in the HHcy group ($P < 0.05$; **Figure 4E**).

Hes1 and Hes5 expression in the olfactory bulb of HHcy mice
In the Wt and ApoE$^{-/-}$ groups, most granule cells were positive for Hes1 and Hes5 and showed an intensity of brown coloration on immunohistochemical analysis (**Figure 5A**). Compared with the Wt and ApoE$^{-/-}$ groups, in the HHcy group, Hes1- and Hes5-positive granule cells were significantly decreased, and most positive cells were light yellow and only few were brown (**Figure 5A**). The number of Hes1- and Hes5-positive granule cells in the HFB group was slightly less compared with that in the Wt and ApoE$^{-/-}$ groups ($P > 0.05$), but significantly more than that in the HHcy group ($P < 0.05$; **Figure 5C**).

As observed through immunofluorescence labeling (**Figure 5B**), a large number of Hes1- and Hes5-positive cells were observed in olfactory bulb sections in the Wt, ApoE$^{-/-}$, and HFB groups. Compared with the Wt, ApoE$^{-/-}$, and HFB groups, in the HHcy group, the number of Hes1- and Hes5-positive cells showed a significant decrease ($P < 0.05$; **Figure 5B**), which was similar to the immunohistochemistry results.
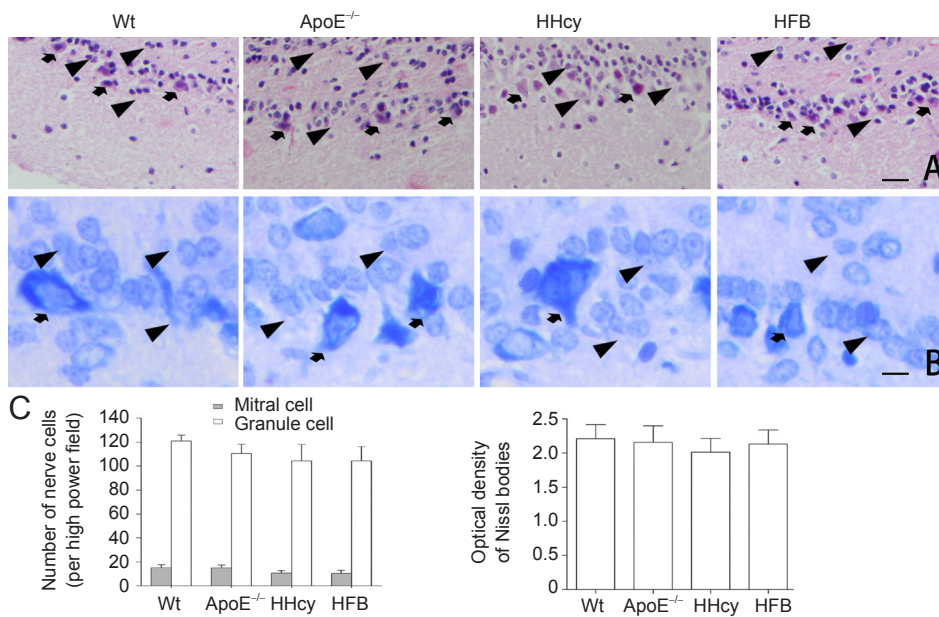
Figure 2 Histological changes in the olfactory bulb of HHcy mice.
(A) Representative histographs in hematoxylin-eosin staining: Normal histology with mitral cells (thick arrows) and granule cells (arrowheads) in Wt, ApoE$^{-/-}$, HHcy, and HFB groups. Scale bar: 50 μm. (B) Representative images of Pischingert staining: Deep blue in mitral cells (thick arrows) and pale blue in granule cells (arrowheads). Scale bar: 10 μm. (C) Quantitative results of the numbers of mitral and granule cells, and the mean optical density of Pischingert staining in the olfactory bulb. Data are expressed as the mean ± SD (n = 12) and analyzed by one-way analysis of variance followed by Tukey's *post-hoc* test for multiple comparisons. The unpaired *t*-test was used between two groups. Wt: Wild-type; ApoE$^{-/-}$: apolipoprotein E-deficient; HHcy: hyperhomocysteinemia; HFB: hyperhomocysteinemia treated with folic acid and vitamin B12.
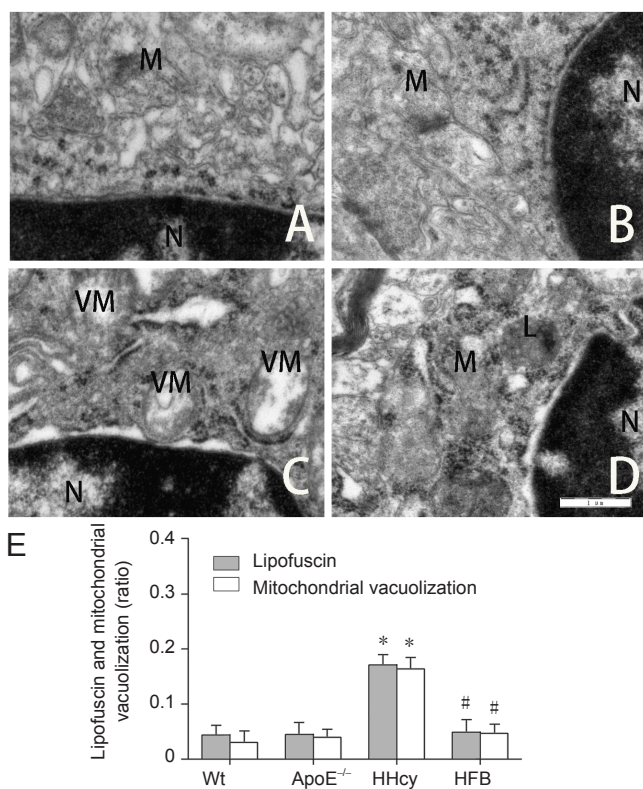
Figure 3 Ultrastructural change in the olfactory bulb of HHcy mice.
(A–D) Transmission electron microscopy images of the olfactory bulb of HHcy mice. (A) Wt group: Mitochondria, rough endoplasmic reticulum, rich ribosome, and nucleus; (B) ApoE$^{-/-}$ group: mitochondria, rough endoplasmic reticulum, and nucleus; (C) HHcy group: mitochondrial vacuolization and nucleus; (D) HFB group: lipofuscin and nucleus. Scale bar: 1 μm. (E) Quantitative results of the cells with mitochondrial vacuolization and lipofuscin. Data are expressed as the mean ± SD (n = 4) and analyzed by one-way analysis of variance followed by Tukey's *post-hoc* test for multiple comparisons. The unpaired *t*-test was used between two groups. *P < 0.05, *vs*. Wt and ApoE$^{-/-}$- groups, respectively; #P < 0.05, *vs*. HHcy group. Wt: Wild-type; ApoE$^{-/-}$: apolipoprotein E-deficient; HHcy: hyperhomocysteinemia; HFB: hyperhomocysteinemia treated with folic acid and vitamin B12; M: mitochondria; N: nucleus; VM: mitochondrial vacuolization; L: lipofuscin.
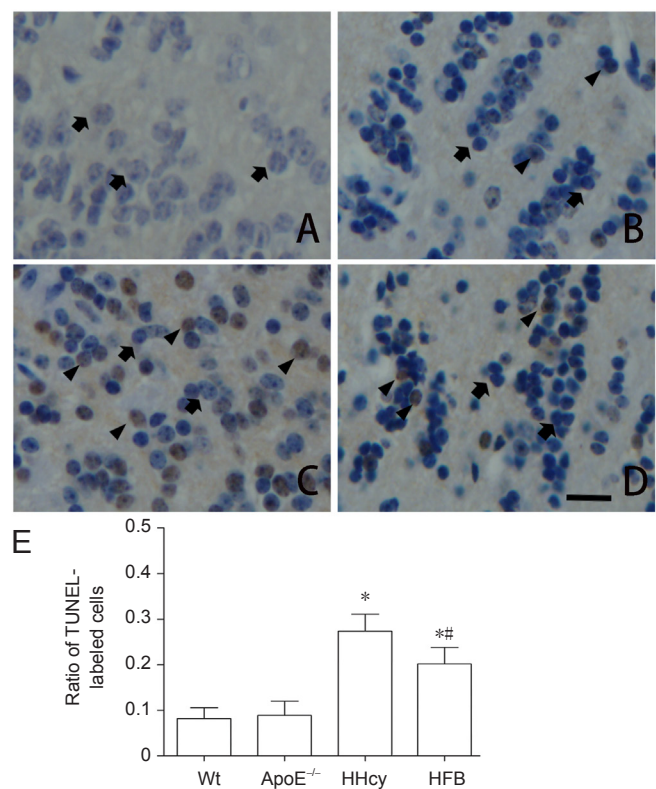

Figure 4 TUNEL-positive granule cells in the olfactory bulb of HHcy mice.
(A–D) TUNEL staining of the olfactory bulb of HHcy mice. (A) Wt group: Granule cells (thick arrows); (B) ApoE$^{-/-}$ group: few scattered TUNEL-positive granule cells (arrowheads); (C) HHcy group: obviously increased TUNEL-positive granule cells (arrowheads); (D) HFB group: few TUNEL-positive granule cells (arrowheads). Scale bar: 30 μm. (E) Quantitative results of TUNEL-positive granule cells. Data are expressed as the mean ± SD (n = 12) and analyzed by one-way analysis of variance followed by Tukey's *post-hoc* test for multiple comparisons. The unpaired *t*-test was used between two groups. *P < 0.05, *vs*. Wt and ApoE$^{-/-}$ groups, respectively; #P < 0.05, *vs*. HHcy group. Wt: Wild-type; ApoE$^{-/-}$: apolipoprotein E-deficient; HHcy: hyperhomocysteinemia; HFB: hyperhomocysteinemia treated with folic acid and vitamin B12; TUNEL: terminal deoxynucleotidyl transferase-mediated dUTP nick end labeling.
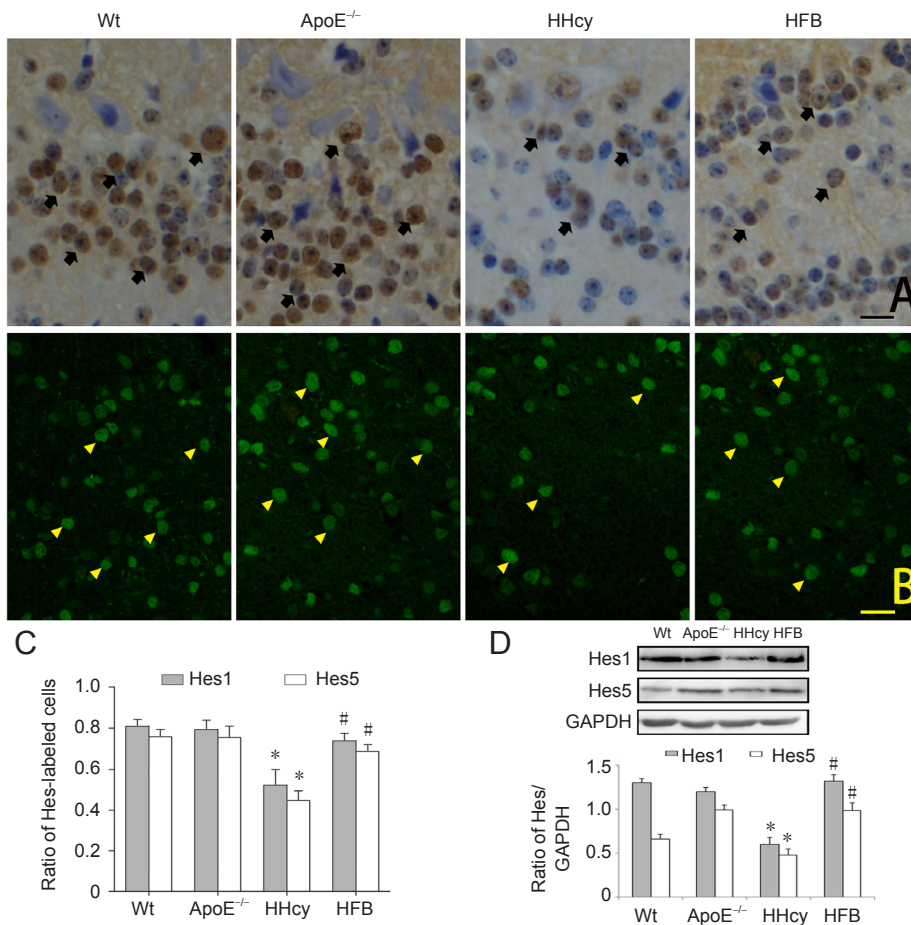
Figure 5 Expression of Hes1 and Hes5 in the olfactory bulb of HHcy mice.
(A) Representative immunohistochemistry of Hes1: In Wt and Apo E$^{-/-}$ groups, most Hes1-immunostained granule cells (thick arrows); in HHcy group, part of Hes1-immunostained granule cells (thick arrows); in HFB group, a few of Hes1-immunostained granule cells (thick arrows). (B) Representative immunofluorescent of Hes5: In Wt, ApoE$^{-/-}$ and HFB groups, most Hes5-labelled granule cells (arrowheads); in HHcy group, decreased Hes5-labelled granule cells (arrowheads). Scale bars in A, B: 20 μm. (C) Numbers of Hes1 and Hes5 immunoreactivated granule cells with (n = 12). (D) Western blot assay of Hes1 and Hes5: The representative western blots and bargraph of relative Hes1 and Hes5 value (n = 8). Data are expressed as the mean ± SD and analyzed by one-way analysis of variance followed by Tukey's *post-hoc* test for multiple comparisons. The unpaired *t*-test was used between two groups. ∗*P* < 0.05, *vs.* Wt and ApoE$^{-/-}$ groups, respectively; #*P* < 0.05, *vs.* HHcy group. Wt: Wild-type; ApoE$^{-/-}$: apolipoprotein E-deficient; HHcy: hyperhomocysteinemia; HFB: hyperhomocysteinemia treated with folic acid and vitamin B12; Hes: hairy enhancer of the split.

Western blot assay of the olfactory bulb is shown in **Figure 5D**. The relative expression of Hes1 and Hes5 in the HHcy group was significantly reduced compared with that in the Wt, ApoE$^{-/-}$, and HFB groups (**Figure 5D**). No significant difference was observed in the amount of protein expression among the Wt, ApoE$^{-/-}$, and HFB groups (*P* > 0.05; **Figure 5D**).

Discussion

The olfactory bulb is a neuronal structure of the vertebrate forebrain that is associated with the olfactory nerve and is involved in olfaction (Lledo et al., 2008; Fletcher et al., 2009). Studies have reported that in the presence of harmful factors, the olfactory bulb acts as an important sensory nerve tissue and may be damaged earlier than many other parts of the brain (Graves et al., 1999; Velayudhan et al., 2013). Velayudhan et al. (2013) suggest that olfactory dysfunction can be used as an important early indicator of neurodegenerative diseases and also as evidence to evaluate disease progression. Graves et al. (1999) indicate that olfactory dysfunction is typically preceded by cognitive impairment. Patients with Alzheimer's disease show the first signs of olfactory dysfunction in motor and memory abnormalities (Velayudhan et al., 2013; Misiak et al., 2017). It remains unclear whether elevated Hcy levels in the blood cause damage to the olfactory bulb in histology and ultrastructure. In the present study, although optical microscopy did not reveal obvious lesions in the histological structure of the olfactory bulb in ApoE$^{-/-}$

mice with moderate HHcy, transmission electron microscopy showed increased lipofuscin and mitochondrial vacuolization associated with HHcy. It is established that more lipofuscin indicates more autophagy in the cells (Kim et al., 2002; Koz et al., 2012; Tripathi et al., 2016). Thus, our results suggest that moderate HHcy induces mitochondrial damage in olfactory bulb neurons, particularly in mitral and granule cells. Moreover, autophagy is involved in the pathogenesis of cardiovascular diseases, aging, and neurodegenerative diseases (Wang et al., 2012; Tripathi et al., 2016; Misiak et al., 2017). These ultrastructural morphological changes might indicate autophagy or mitophagy, thus facilitating the understanding of mechanisms underlying HHcy-induced neural damages (Kim et al., 2002).

The mechanisms underlying central nervous system injury induced by HHcy are poorly understood (Curro et al., 2014; Xu et al., 2017). Hcy can serve as excitatory amino acids to increase the sensitivity of neurons to exogenous pathogenies and oxidative stress (Koz et al., 2012; Curro et al., 2014; Qasim et al., 2016). Some studies have suggested that HHcy exacerbates the cellular sensitivity to oxidative damage and induces excitotoxicity associated with the glutamate receptor subtype and N-methyl-D-aspartate activation (Wang et al., 2012; Curro et al., 2014; Veeranki et al., 2015; Tripathi et al., 2016). DNA damage may result in P53 activation and mitochondrial dysfunction (Koz et al., 2012; Veeranki et al., 2015; Qasim et al., 2016). In cultured SH-SY5Y neuroblastoma

cell, the production of reactive oxygen species was increased by 4.4 folds after 5 days of Hcy exposure. Longer exposure to Hcy (> 5 days) can produce genotoxic effects, such as DNA fragmentation (Curro et al., 2014). It is indicated that apoptosis is induced by elevated Hcy in cardiac and cerebral cells (Tyagi et al., 2010; Wan et al., 2011; Wang et al., 2012). Our results revealed that in the HHcy group, TUNEL-positive cells in the granule cell layer of the olfactory bulb increased markedly compared with the mice without HHcy from the Wt group and ApoE$^{-/-}$ group. This result suggests that moderate HHcy induces the apoptosis of granule cells and interneurons in the olfactory bulb, as well as a decrease in the regeneration and function of the olfactory bulb. Similar results have been reported in the brains of adult and pregnant rats (Koz et al., 2012; Wang et al., 2012). Meanwhile, *in vitro* experiments demonstrated that HHcy may obviously restrain cardiac stem cell-mediated cardiac repair after myocardial infarction in rats (Wan et al., 2011). It is established that neuronal regeneration is complex and involves proliferation, signal transduction, and expression of many related genes (Blackshaw et al., 2010; Imayoshi et al., 2010; Aujla et al., 2013).

The Notch signaling pathway, which regulates the signal recognition of cells, is one of the important pathways to regulate neuronal stem cell proliferation, differentiation, and self-renewal, as well as to maintain intracellular environment stability (Fortini, 2009; Imayoshi et al., 2010; Weber et al., 2014). After binding to its ligand, the Notch receptor undergoes tumor necrosis factor-α-converting enzyme cleavage and PS1-dependent γ-secretase, releasing the Notch intracellular domain with the nuclear localization signal, entering the nucleus, and associating with RBP-Jk. Moreover, binding of the RAM domain to anchor on the Notch intracellular domain activates the downstream basic helix-loop-helix family of transcriptional repressors Hes1 and Hes5 and initiates transcription (Aujla et al., 2013; Weber et al., 2014). In this study, a significantly decreased expression of Hes1 and Hes5 was observed in the olfactory bulb of the HHcy group, which was quantified by western blot assay or determined in localization through immunohistochemistry and immunofluorescence. Our results suggest that HHcy-induced neuronal apoptosis, lipofuscin, and mitochondrial vacuolization in olfactory bulb are associated with the low expression of Hes1 and Hes5. The role of Hes1 and Hes5 in the generation and regeneration of adult olfactory bulb neurons is unclear. Neuronal stem cells have been reported to be unable to activate or proliferate in the dormant state after Notch1 knockout (Katoh and Katoh, 2007; Del Debbio et al., 2010; Shimojo et al., 2011). When RBJk was knocked out, neuronal stem cells could proliferate in a short time and then rapidly differentiate into neurons, leading to the premature exhaustion of neuronal stem cells (Del Debbio et al., 2010; Shimojo et al., 2011). However, as the vulnerable brain region, the significance of low Hes1 and Hes5 expression induced by HHcy in the olfactory bulb is unclear, may be associated with the regenerative potency or neurogenesis, and should be further investigated. HHcy-induced neuronal excitatory effects and amino acid metabolic disorders may be related to cognitive

impairment (Gao et al., 2012; Koz et al., 2012), atherosclerosis (Imayoshi et al., 2010; Shimojo et al., 2011; Weber et al., 2014), dementia, depression, learning (Troen et al., 2008; Koz et al., 2012) and memory capacity decline, as well as to Alzheimer's and Parkinson's disease (Velayudhan et al., 2013; Ganguly and Alam, 2015; Kamat et al., 2016; Misiak et al., 2017). They may also be associated with the downregulation of Hes1 and Hes5 expression in neurons. Although the regeneration of nerve or neurons is regulated in a large number of genes, the downregulation of Hes1 and Hes5, as an important regulator of stem cell proliferation and differentiation, may be associated with decreased neuronal regeneration (Blackshaw et al., 2010; Imayoshi et al., 2010; Aujla et al., 2013). However, many problems require further investigation, such as how HHcy induces low Hes1 and Hes5 expression to reduce neuronal regeneration potential.

A limitation of the present study is that the results only provide evidence on histology, ultrastructure, and Nissl body in olfactory bulb neurons, as well as Hes1 or Hes5 expression during HHcy. To determine the effect of HHcy on the brain, aforementioned changes at different HHcy levels, and proliferation involved in the downregulation of Hes1 or Hes5, the Notch-Hes pathway and its relative gens with HHcy could be further investigated.

In summary, moderate HHcy was induced in ApoE$^{-/-}$ mice by feeding them a high-methionine diet. The histological and histochemical examination of the olfactory bulb showed no significant structural abnormalities in the HHcy group, but revealed an increased number of TUNEL-positive granule cells. Ultrastructural observation showed markedly increased lipofuscin and mitochondrial vacuolization in the mice with moderate HHcy. Immunohistochemistry and western blot assay revealed that Hes1 and Hes5 expression was obviously decreased in the HHcy group compared with that in the mice without HHcy from the Wt group and ApoE$^{-/-}$ group. These results suggest that moderate HHcy causes mitochondrial injury in the olfactory bulb neurons of ApoE$^{-/-}$ mice, induces the mitophagy and apoptosis of granule cells, and inhibits neuronal regeneration, and may be involved in the downregulation of Hes1 and Hes5 expression.

References

Aléssio AC, Santos CX, Debbas V, Oliveira LC, Haddad R, Annichino-Bizzacchi JM (2011) Evaluation of mild hyperhomocysteinemia during the development of atherosclerosis in apolipoprotein E-deficient and normal mice. Exp Mol Pathol 90:45-50.

Aujla PK, Naratadam GT, Xu L, Raetzman LT (2013) Notch/Rbpjkappa signaling regulates progenitor maintenance and differentiation of hypothalamic arcuate neurons. Development 140:3511-3521.

Blackshaw S, Scholpp S, Placzek M, Ingraham H, Simerly R, Shimogori T (2010) Molecular pathways controlling development of thalamus and hypothalamus: from neural specification to circuit formation. J Neurosci 30:14925-14930.

Curro M, Gugliandolo A, Gangemi C, Risitano R, Ientile R, Caccamo D (2014) Toxic effects of mildly elevated homocysteine concentrations in neuronal-like cells. Neurochem Res 39:1485-1495.

Del Debbio CB, Balasubramanian S, Parameswaran S, Chaudhuri A, Qiu F, Ahmad I (2010) Notch and Wnt signaling mediated rod photoreceptor regeneration by Muller cells in adult mammalian retina. PLoS One 5:e12425.

Fletcher ML, Masurkar AV, Xing J, Imamura F, Xiong W, Nagayama S, Mutoh H, Greer CA, Knöpfel T, Chen WR (2009) Optical imaging of postsynaptic odor representation in the glomerular layer of the mouse olfactory bulb. J Neurophysiol 102:817-830.

Fortini ME (2009) Notch signaling: the core pathway and its posttranslational regulation. Dev Cell 16:633-647.

Gall CM, Hendry SH, Seroogy KB, Jones EG, Haycock JW (1987) Evidence for coexistence of GABA and dopamine in neurons of the rat olfactory bulb. J Comp Neurol 266:307-318.

Ganguly P, Alam SF (2015) Role of homocysteine in the development of cardiovascular disease. Nutr J 14:6.

Gao L, Zeng XN, Guo HM, Wu XM, Chen HJ, Di RK, Wu Y (2012) Cognitive and neurochemical alterations in hyperhomocysteinemic rat. Neurol Sci 33:39-43.

Graves AB, Bowen JD, Rajaram L, McCormick WC, McCurry SM, Schellenberg GD, Larson EB (1999) Impaired olfaction as a marker for cognitive decline: interaction with apolipoprotein E epsilon4 status. Neurology 53:1480-1487.

Imayoshi I, Sakamoto M, Yamaguchi M, Mori K, Kageyama R (2010) Essential roles of Notch signaling in maintenance of neural stem cells in developing and adult brains. J Neurosci 30:3489-3498.

Jiang Y, Zhang H, Sun T, Wang J, Sun W, Gong H, Yang B, Shi Y, Wei J (2012) The comprehensive effects of hyperlipidemia and hyperhomocysteinemia on pathogenesis of atherosclerosis and DNA hypomethylation in ApoE$^{-/-}$ mice. Acta Biochim Biophys Sin (Shanghai) 44:866-875.

Jing L, He Q, Zhang JZ, Li PA (2013) Temporal profile of astrocytes and changes of oligodendrocyte-based myelin following middle cerebral artery occlusion in diabetic and non-diabetic rats. Int J Biol Sci 9:190-199.

Kamat PK, Kyles P, Kalani A, Tyagi N (2016) Hydrogen sulfide ameliorates homocysteine-induced Alzheimer's disease-like pathology, blood-brain barrier disruption, and synaptic disorder. Mol Neurobiol 53:2451-2467.

Katoh M, Katoh M (2007) Integrative genomic analyses on HES/HEY family: Notch-independent HES1, HES3 transcription in undifferentiated ES cells, and Notch-dependent HES1, HES5, HEY1, HEY2, HEYL transcription in fetal tissues, adult tissues, or cancer. Int J Oncol 31:461-466.

Kim JM, Lee H, Chang N (2002) Hyperhomocysteinemia due to short-term folate deprivation is related to electron microscopic changes in the rat brain. J Nutr 132:3418-3421.

Koz ST, Etem EO, Baydas G, Yuce H, Ozercan HI, Kuloglu T, Koz S, Etem A, Demir N (2012) Effects of resveratrol on blood homocysteine level, on homocysteine induced oxidative stress, apoptosis and cognitive dysfunctions in rats. Brain Res 1484:29-38.

Lledo PM, Merkle FT, Alvarez-Buylla A (2008) Origin and function of olfactory bulb interneuron diversity. Trends Neurosci 31:392-400.

Misiak M, Vergara Greeno R, Baptiste BA, Sykora P, Liu D, Cordonnier S, Fang EF, Croteau DL, Mattson MP, Bohr VA (2017) DNA polymerase beta decrement triggers death of olfactory bulb cells and impairs olfaction in a mouse model of Alzheimer's disease. Aging cell 16:162-172.

Nichol D, Shawber C, Fitch MJ, Bambino K, Sharma A, Kitajewski J, Stuhlmann H (2010) Impaired angiogenesis and altered Notch signaling in mice overexpressing endothelial Egfl7. Blood 116:6133-6143.

Qasim M, Bukhari SA, Ghani MJ, Masoud MS, Huma T, Arshad M, Haque A, Ibrahim Z, Javed S, Rajoka MI (2016) Relationship of oxidative stress with elevated level of DNA damage and homocysteine in cardiovascular disease patients. Pak J Pharm Sci 29:2297-2302.

Reule CA, Goyvaerts B, Schoen C (2017) Effects of an L-arginine-based multi ingredient product on endothelial function in subjects with mild to moderate hypertension and hyperhomocysteinemia - a randomized, double-blind, placebo-controlled, cross-over trial. BMC Complement Altern Med 17:92.

Shimojo H, Ohtsuka T, Kageyama R (2011) Dynamic expression of notch signaling genes in neural stem/progenitor cells. Front Neurosci 5:78.

Tripathi M, Zhang CW, Singh BK, Sinha RA, Moe KT, DeSilva DA, Yen PM (2016) Hyperhomocysteinemia causes ER stress and impaired autophagy that is reversed by vitamin B supplementation. Cell Death Dis 7:e2513.

Troen AM, Shea-Budgell M, Shukitt-Hale B, Smith DE, Selhub J, Rosenberg IH (2008) B-vitamin deficiency causes hyperhomocysteinemia and vascular cognitive impairment in mice. Proc Natl Acad Sci U S A 105:12474-12479.

Tyagi N, Vacek JC, Givvimani S, Sen U, Tyagi SC (2010) Cardiac specific deletion of N-methyl-d-aspartate receptor 1 ameliorates mtMMP-9 mediated autophagy/mitophagy in hyperhomocysteinemia. J Recept Signal Transduct Res 30:78-87.

Veeranki S, Lominadze D, Tyagi SC (2015) Hyperhomocysteinemia inhibits satellite cell regenerative capacity through p38 alpha/beta MAPK signaling. Am J Physiol Heart Circ Physiol 309:H325-334.

Velayudhan L, Pritchard M, Powell JF, Proitsi P, Lovestone S (2013) Smell identification function as a severity and progression marker in Alzheimer's disease. Int Psychogeriatr 25:1157-1166.

Wan J, Deng Y, Guo J, Xiao G, Kuang D, Zhu Y, Duan Y, Wang G (2011) Hyperhomocysteinemia inhibited cardiac stem cell homing into the peri-infarcted area post myocardial infarction in rats. Exp Mol Pathol 91:411-418.

Wang J, Ge J, Yang L, Zhang H, Li X, Xue D (2012) Brain cell apoptosis and enhancement of nervous excitability in pregnant rats with high plasma levels of homocysteine. Neural Regen Res 7:2199-2205.

Weber D, Wiese C, Gessler M (2014) Hey bHLH transcription factors. Curr Top Dev Biol 110:285-315.

Xu B, Kong X, Xu R, Song Y, Liu L, Zhou Z, Gu R, Shi X, Zhao M, Huang X, He M, Fu J, Cai Y, Li P, Cheng X, Wu C, Chen F, Zhang Y, Tang G, Qin X, et al. (2017) Homocysteine and all-cause mortality in hypertensive adults without pre-existing cardiovascular conditions: Effect modification by MTHFR C677T polymorphism. Medicine (Baltimore) 96:e5862.